Neuron
Article

Neural Oscillations and Synchronization Differentially Support Evidence Accumulation in Perceptual and Value-Based Decision Making

Rafael Polanía,[1,*] Ian Krajbich,[2,3] Marcus Grueschow,[1] and Christian C. Ruff[1,*]
[1]Laboratory for Social and Neural Systems Research (SNS-Lab), Department of Economics, University of Zurich, CH-8006 Zurich, Switzerland
[2]Department of Psychology
[3]Department of Economics
The Ohio State University, Columbus, OH 43210, USA
*Correspondence: rafael.polania@econ.uzh.ch (R.P.), christian.ruff@econ.uzh.ch (C.C.R.)
http://dx.doi.org/10.1016/j.neuron.2014.03.014

SUMMARY

Organisms make two types of decisions on a regular basis. Perceptual decisions are determined by objective states of the world (e.g., melons are bigger than apples), whereas value-based decisions are determined by subjective preferences (e.g., I prefer apples to melons). Theoretical accounts suggest that both types of choice involve neural computations accumulating evidence for the choice alternatives; however, little is known about the overlap or differences in the processes underlying perceptual versus value-based decisions. We analyzed EEG recordings during a paradigm where perceptual- and value-based choices were based on identical stimuli. For both types of choice, evidence accumulation was evident in parietal gamma-frequency oscillations, whereas a similar frontal signal was unique for value-based decisions. Fronto-parietal synchronization of these signals predicted value-based choice accuracy. These findings uncover how decisions emerge from topographic- and frequency-specific oscillations that accumulate distinct aspects of evidence, with large-scale synchronization as a mechanism integrating these spatially distributed signals.

INTRODUCTION

In animals and humans, goal-directed behavior involves the planning of motor actions based on sensory information about the environment and the organism's internal state. How exactly these motor actions are selected in the presence of two or more choice alternatives is still unknown and has become a central question in neuroscience. Theoretical models and empirical work propose that this process—known as decision-making—involves the continuous accumulation of sensory evidence until a decision criterion is met and a motor action is executed (Gold and Shadlen, 2007). Computational models—such as sequential sampling models (SSMs)—suggest that these evidence accumulation (EA) computations constitute a domain-general decision mechanism (Bogacz et al., 2006; Gerstner et al., 2012; Smith and Ratcliff, 2004; Usher and McClelland, 2001). However, SSMs have so far mostly been applied to choices based on objective information about physical properties of sensory stimuli (perceptual decision making [PDM]) (Bode et al., 2012; Bowman et al., 2012; Brunton et al., 2013; Deco et al., 2010; Ossmy et al., 2013; Ratcliff et al., 2009; van Vugt et al., 2012; White et al., 2012). Comparatively few studies have employed SSMs to investigate other types of decisions that pervade everyday life, such as choices based on the participant's subjective preferences (value-based decision making [VDM]) (Hunt et al., 2012; Krajbich and Rangel, 2011; Krajbich et al., 2010; Milosavljevic et al., 2010; Philiastides and Ratcliff, 2013). Crucially, while there are good theoretical reasons to believe that common mechanisms should underlie both PDM and VDM (Summerfield and Tsetsos, 2012), it has been difficult to compare these two types of choices due to major differences in the experimental approaches and sensory stimuli employed for these two streams of research. It is thus unclear whether a common EA process underlies both types of decision making.

In the present study, we identify electrophysiological markers of EA processes that were derived using a SSM fitted to participants' choice data and directly compare them between perceptual- and value-based choices. To this end, we developed a behavioral paradigm where, while we acquired EEG recordings, participants performed perceptual- and value-based decisions using the same sensory stimuli and motor outputs. With this experiment we were thus able to control for the various differences that would normally prevent direct comparisons between the cortical computations involved in PDM and VDM paradigms.

In our study, we record neural activity using EEG, as this technique allows noninvasive, parallel, and temporally precise recording of multiple cortical areas in healthy human volunteers. The importance of parietal and prefrontal regions for evidence integration in PDM (and possibly VDM) has been established by pioneering monkey electrophysiology studies using invasive single-unit recordings in various areas (e.g., for LIP, Churchland

et al., 2008; Kiani and Shadlen, 2009; Shadlen and Newsome, 2001; for FEF, Kim and Shadlen, 1999). These studies have typically been conducted in the monkey brain and have often recorded from neurons in a single location at a time, leaving it unclear whether parallel evidence integration processes occur in multiple cortical areas of the human brain and how such processes are integrated to yield the final choice outcome. However, recent EEG investigations (Kelly and O'Connell, 2013; O'Connell et al., 2012) of PDM showed that it is possible to simultaneously capture parallel decision formation and motor preparatory signals in parietal and motor regions, respectively. This and other recent studies demonstrate that EEG (and magnetoencephalograpy [MEG]) can noninvasively reveal multiple neural determinants of decision formation in the human brain (Donner et al., 2009; Hunt et al., 2012; O'Connell et al., 2012; Wyart et al., 2012).

In our investigation of neural evidence integration during PDM and VDM, we focus on neural oscillations in the gamma-frequency band, as such signals should carry information related to the synchronous activity of multiple groups of cortical neurons (Bollimunta and Ditterich, 2012; Buzsáki et al., 2012; Donner and Siegel, 2011; Polanía et al., 2012a). Single-unit recording studies have so far reported monotonically increasing firing rates in integrator regions until a motor action is executed (Huk and Shadlen, 2005; Shadlen and Newsome, 2001), and a recent EEG study of PDM based on slowly varying sensory stimuli showed a monotonically rising event-related potential (ERP) signal that may correspond to such firing-rate increases (O'Connell et al., 2012). Computational models suggest that such phenomena emerge by recurrent excitation mediated by NMDA receptors and feedback inhibition, which together amplify the difference between conflicting inputs (Wang, 2002). Such coordinated excitation and inhibition has repeatedly been shown to result in gamma activity (neural oscillations at 30–90 Hz) that can be detected with extracellular recordings (Bollimunta and Ditterich, 2012; Buzsáki and Wang, 2012). Thus, we hypothesize that these stereotypical increases in firing rates (or ERPs) in integrator regions during the decision-making process are reflected in modulations of gamma power that can be captured noninvasively using our EEG recordings.

Our behavioral paradigm allowed us to compute for every trial the amount of perceptual- or value-based evidence for each choice alternative and to fit a simple SSM to the behavioral data. This model accounted well for behavioral performance and allowed us to derive trial-specific predicted EA signals for both types of choice. These model-based EA signals accurately predicted EEG traces related to (1) specific time-frequency gamma power modulations in parietal regions for both PDM and VDM, (2) similar gamma power modulations in fronto-polar regions specifically during the VDM task, and (3) motor preparatory signals. Crucially, gamma phase coupling between the fronto-polar and parietal regions was higher for VDM than for PDM and was predictive of correct value-based decisions. Taken together, these results support the idea that both PDM and VDM involve computationally similar EA processes implemented in distinct cortical areas. These oscillatory EA processes occur in a quasi-parallel fashion and are mediated by both local and large-scale oscillatory synchronization.

RESULTS

Behavior

We recorded 128-channel EEG data from hungry, healthy human volunteers performing our binary decision-making task (see Experimental Procedures for details). Before performing the decision-making task, we asked the participants to provide subjective perceptual- and value-based ratings for a set of food images. For value-based ratings, participants indicated "how much they wanted to eat the presented food snack at the end of the experiment" (Krajbich and Rangel, 2011; Krajbich et al., 2010). For perceptual-based ratings, we asked the participants to provide an estimate of "how much they thought (in percent) the food item was covering the black background within the white square" (see Experimental Procedures; Figure 1A; Figure S1 available online). These subjective perceptual ratings were highly accurate, as they were strongly correlated with the objective size measurements for all subjects ($T(17) = 42.4$, $p < 10^{-15}$; Figure S1). Moreover, a comparison of accuracies estimated for each subject based on either subjective or objective perceptual ratings revealed no significant difference ($T(17) = 1.55$, $p > 0.13$).

For the main experiment, we generated a balanced set of PDM and VDM trials divided into four different difficulty levels, based on the individual subjective ratings of each participant. Importantly, the perceptual- and value-based ratings provided by the participants were not correlated ($T(17) = 0.24$, $p > 0.8$; Figure S1), demonstrating that we could examine PDM and VDM based on identical visual stimuli in a fully independent fashion.

Immediately after providing the ratings, subjects performed perceptual- and value-based decisions based on the same set of naturalistic visual stimuli and involving identical motor outputs. The only difference between both types of decisions was which type of evidence needed to be accumulated for the choice (perceptual or value based; Figure 1A). In the VDM task, subjects indicated which item they would prefer to receive at the end of the experiment, while in the PDM task, subjects indicated which item covered more of its background. In both tasks, we define a correct choice as a trial in which the subject chose the item with a higher rating from the separate rating tasks (Experimental Procedures).

Our behavioral results revealed that our experimental design allowed a clear computational separation of PDM and VDM: reaction times (RTs) and accuracies during both types of choice were only influenced by the corresponding type of evidence (i.e., perceptual for PDM and value-based for VDM) (Figures 1B–1D). Control analyses confirmed that there were no confounding effects of presentation side (subjects performed equally well when the food items were presented either to the left or right side of the screen; t test on mean accuracies and RTs: $T(17) < 1.1$, $p > 0.3$). Taken together, these results show that our paradigm is well suited to directly compare PDM and VDM, as both types of decisions were taken in a fully independent fashion and reflected selective accumulation of just one type of evidence.

Model, Fits, and Predictions

To predict the neural dynamics of EA in the human brain, we fitted a dynamical SSM of decision making to the behavioral

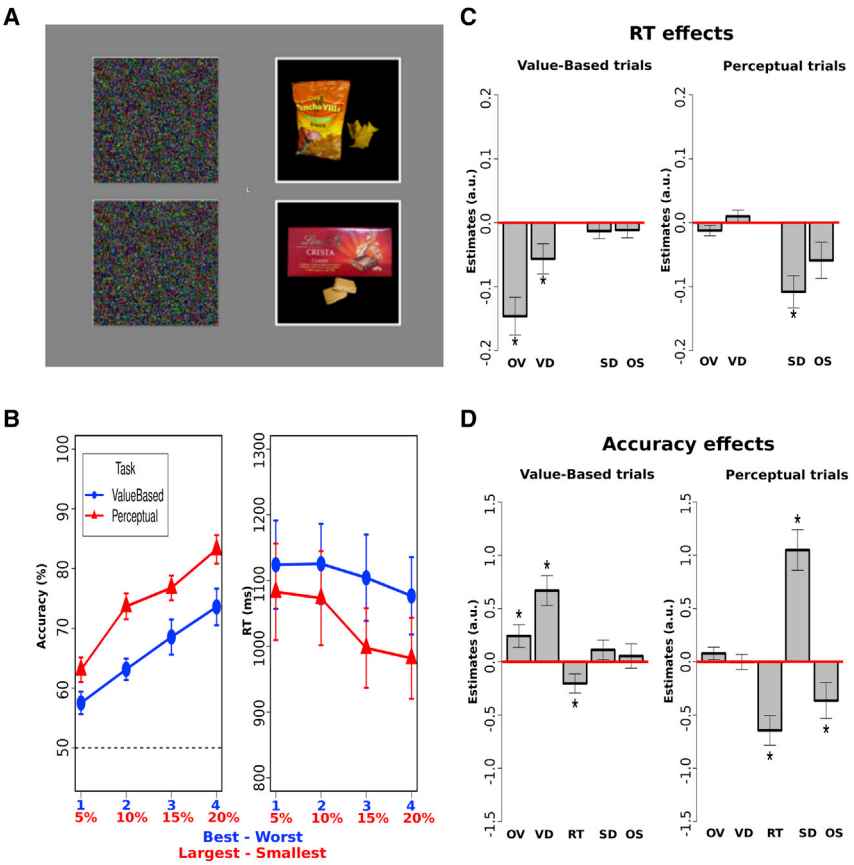

Figure 1. Paradigm and Behavior

(A) Example screenshot during the decision stage. Participants were always cued about the type of trial (PDM or VDM) and on which side of the screen the food items would be presented (right in this example, always one stimulus above and one below). On the opposite side of the screen, an average-scrambled image of the two food items was displayed in order to avoid spatial imbalance (see Experimental Procedures). In VDM trials, subjects chose which item (the upper or the lower item) they preferred to eat at the end of the experiment. In PDM trials, subjects chose which item covered more of the black background.

(B) Accuracies (left panel) and reaction times for correct trials (right panel) are shown for each evidence level of the VDM (blue) and PDM (red) tasks. Longer RTs and lower accuracy levels show that participants were behaviorally sensitive to the evidence manipulation.

(C and D) Behavior was only influenced by the evidence relevant for the current task (i.e., perceptual for PDM and value-based for VDM). Bar plots represent mean standardized estimates across subjects from multiple regressions of (C) reaction times and (D) accuracies on the overall value (OV) (sum of both items), value difference (VD) between both items, overall size (OS) (sum of both items), size difference (SD) between both items, and the reaction time (RT) in the present trial. Error bars represent SEM. *$p < 0.05$. See also Figure S1.

data of our participants. As perceptual- and value-based decisions were taken in a fully independent fashion and reflected selective accumulation of just one type of evidence (see Figures 1C and 1D), we could fit a single SSM to both tasks (PDM or VDM) and only needed to change the input to this model from trial to trial. For any given choice, the model therefore received task difficulty of the currently relevant stimulus dimension as input (i.e., $I_{PDM} = |S_1 - S_2|$ and $I_{VDM} = |V_1 - V_2|$, where S and V are the rated sizes and values of the items on each PDM and VDM trial, respectively). Based on these inputs, the model then (1) accounted for both accuracies and RTs for each trial type and (2) provided us with a prediction of the moment-by-moment accumulated evidence signal (at a millisecond resolution) until a decision was made.

For this SSM approach, we used the general form of the Ornstein-Uhlenbeck process (OU) (Experimental Procedures), which can be described as a reduction of the leaky competing accumulator family of models (Bogacz et al., 2006). In brief, the OU is described by the following equation:

$$dEA = (\lambda \times EA + kI)dt + \sigma dW, \quad (1)$$

where *EA* is the amount of evidence accumulated at a given time *t* (i.e., the moment-by-moment evidence favoring one of the alternatives), *I* is the input to the system (i.e., difference in value or relative size between the food items $I_{PDM} = |S_1 - S_2|$ and $I_{VDM} = |V_1 - V_2|$, where *S* and *V* are the rated sizes and values of the items on each PDM and VDM trial, respectively), *k* is a linear drift parameter that scales the input (in units of ms^{-1}), λ is a parameter that denotes the leak-strength (or urgency) of the process, and σdW are independent white noise (Wiener) increments of step σ (sampled independently every 1 ms). Additionally, we accounted for visual processing and cortico-muscular responses by subtracting a non-decision time (*nDT*, also a parameter to be fitted) from the empirical RTs. By fitting this model to the observed behavioral data, we could therefore generate a prediction for a likely neural EA signal underlying observed behavior, given the model and its input on a given trial.

Initially, we fitted the model (Equation 1) to the individual data of each participant and compared the fitted parameters for the two decision types. This analysis revealed that the only parameter that differed between PDM and VDM across subjects was the drift parameter *k*. This drift parameter adjusts the impact of the input *I* (e.g., value or size difference) on the evolution of the EA signals (Figure S2A). We found that *k* was larger in PDM than in VDM (to make *k* comparable between PDM and VDM in this specific analysis, the input *I* to the model, Equation 1, ranged from 1 to 4 in unitary steps for each difficulty level) (i.e., $I \in [1, 2, 3, 4]$ for both PDM and VDM) (see Figure S2A). This means that subjects accumulated evidence at a higher rate in PDM than in VDM, for the specific value and size differences used in our task (note that this does not necessarily represent any fundamental difference between PDM and VDM, but rather that the value and size differences in the two tasks were not perfectly matched on difficulty) (see Experimental Procedures; Figures

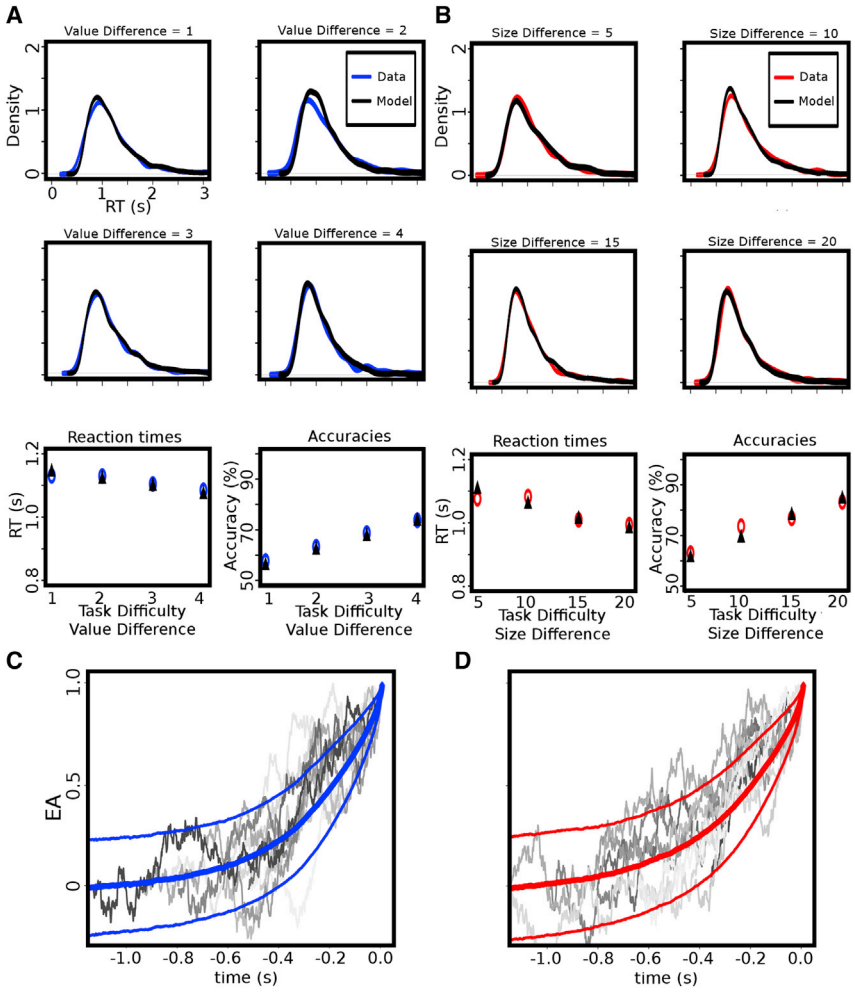

Figure 2. Model Fits and Predictions

(A and B) The OU model provided excellent fits to observed choices and reaction times in the (A) VDM task and (B) PDM task. The first two rows in (A) and (B) show density plots of the RTs for correct trials at each difficulty level (value difference levels in VDM and size difference levels in PDM) (see Figure 1B), and the last row shows mean accuracies and RTs for both data and model.

(C and D) Fitted parameters of the OU model were used to generate model predictions of the decision variable for VDM ([C], blue) and PDM ([D], red). Grey traces in each panel are randomly selected simulated trials of the OU process time locked to boundary crossing. The thick blue/red line represents the mean of 5,000 simulated trials time locked to model response. Thin blue/red lines above and below the thicker line represents ±SD. These model predictions were tested against time-frequency decompositions of our collected EEG data. See also Figure S3.

1B and S2A). Importantly, our analysis clearly indicates that behavioral differences between the two tasks were not driven by differences in noise (parameter σ) or urgency (parameter λ).

In order to derive the model-predicted EA signal for the EEG analyses, we then fitted the model to the data pooled across participants to ensure the maximum amount of precision for parameter estimation (Figure S2B; see also Hare et al., 2011; Krajbich et al., 2010). The resulting model parameters were as follows: $\lambda = 2.3$, $k = 0.11$ (ms^{-1}), $\sigma = 0.6$, and $nDT = 0.4$ s for VDM with inputs $I = VD \in [1, 2, 3, 4]$ and $\lambda = 1.8$, $k = 0.04$ (ms^{-1}), $\sigma = 0.7$, and $nDT = 0.4$ s for PDM with inputs $I = SD \in$ [5%, 10%, 15%, 20%] (inspection of the likelihood landscape confirms that we found a global maximum; see Experimental Procedures and Figure S2 for further details and discussion of the model fits). The model provided excellent fits for accuracies and RTs in both tasks (Figures 2A and 2B) and led to a predicted response-locked EA signal depicted in Figures 2C and 2D. Note that for PDM trials, this predicted EA signal is identical if we used the subjective ratings instead of the objective sizes of the items as input to the model (Figure S2C). Note also that the exponential-like shape of the model-predicted EA signals was not caused by the urgency signal in the OU model fits (i.e., $\lambda > 0$), as such a shape was also present for fits of a standard DDM to our data (i.e., $\lambda = 0$ in Equation 1; Figure S2D) (see also Ratcliff et al., 2003) or even for $\lambda < 0$ (Schurger et al., 2012). In the EEG analyses, we then inspected the time-frequency decompositions of our collected EEG data for any signals that closely followed these model-predicted, response-locked EA signals.

Local Oscillations Encode the Model-Predicted EA Signal

As briefly discussed in the introduction, we hypothesized that stereotypical increases of firing rates in integrator regions—previously reported in single-unit and EEG-ERP recording studies (O'Connell et al., 2012; Shadlen and Newsome, 2001)—are reflected in modulations of time-frequency gamma power that can be captured using EEG recordings in humans. We tested this hypothesis by relating the model-predicted EA signals to time-frequency decompositions of the EEG data, time-locked to the response (Experimental Procedures). Note that for all these analyses, we ruled out artificial modulations of gamma power by possible "stereotypical" eye movements with control analyses of eye-tracking data (Supplemental Experimental Procedures).

In our analysis, trials were divided into even and odd trials in order to test predictions of the fitted model out of sample (i.e., against independent data). To this end, we first used the even-numbered trials to identify sensors where oscillatory activity was closely related to the shape of the model-predicted EA, and then we formally tested the model predictions with the data from the independent odd-numbered trials. For the first step, we linearly regressed time-frequency decompositions of the even trials against the model-predicted EA signal. We only considered clusters in the sensor-frequency space where this yielded significant results surviving correction for multiple

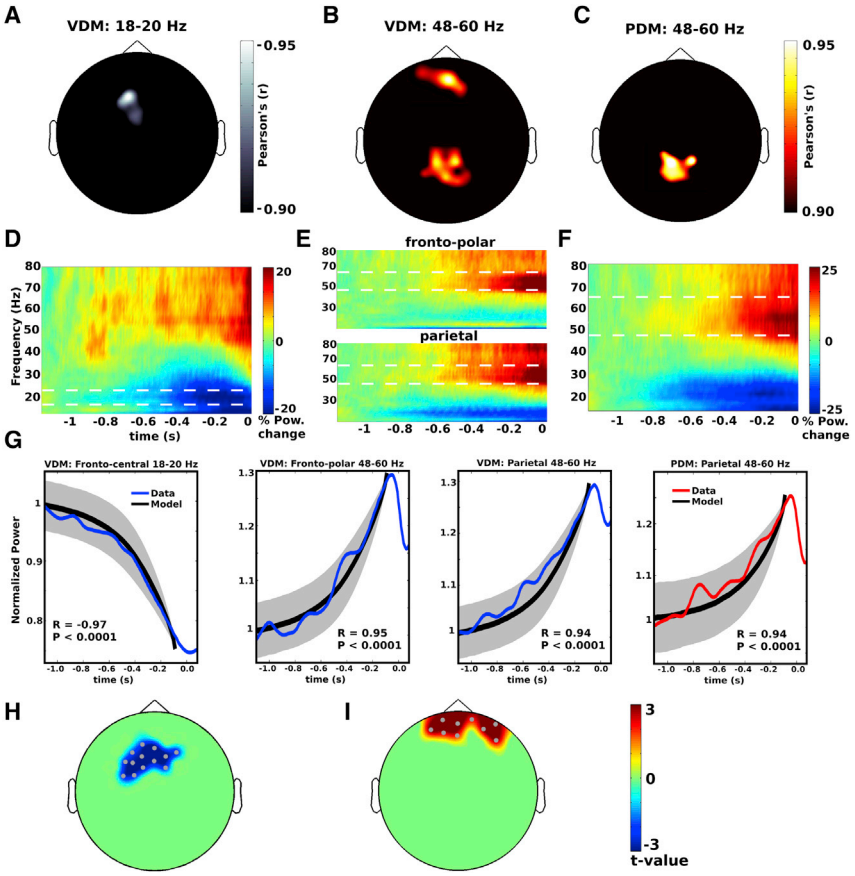

Figure 3. Relationship between EEG Time-Frequency Decompositions and Model Predictions

Time-frequency decompositions were divided into even and odd trials in order to test model predictions out of sample.

(A–C) Clusters in sensor-frequency space where, during even-numbered trials, neural oscillations were related to model predictions (see Experimental Procedures and Results).

(D–F) Normalized time-frequency decompositions averaged across sensors within the clusters that closely followed the model-predicted EA signal (see topographical maps in [A]–[C]). The white dashed lines in the time frequency decompositions bracket the frequency range corresponding to the topographical plots shown in (A)–(C).

(G) In order to test our model predictions out of sample, we investigated the relationship between the model and the other half of the data (odd-numbered trials) based on the sensor-frequency clusters shown in (A)–(C). Colored lines correspond to average time-frequency decompositions of the data from odd-numbered trials, extracted from the sensor-frequency clusters (defined with data from even-numbered trials) shown in (A)–(C). Grey shaded areas correspond to ±1 SD of the model-predicted EA.

(H–I) Compare the relationship of model predictions and data between conditions (VDM versus PDM) via a t statistic of the difference in model-data correlation between conditions for each EEG channel and each frequency band.

(H) Negative correlations of the model predictions with beta-band oscillations were stronger for VDM than PDM at fronto-central sensors (cluster spanning 18–23 Hz).

(I) Positive correlations of model predictions with gamma-band oscillations were stronger for VDM than PDM at fronto-polar sensors (cluster spanning 48–65 Hz). Clusters in (H) and (I) survive Monte-Carlo cluster correction for multiple comparisons at $p < 0.05$. See also Figure S3.

comparisons and where time-frequency decompositions for each time-point lay within 1 SD of the model predictions (Experimental Procedures).

Our analysis revealed that, in both PDM and VDM trials, model-predicted neural EA signals were present in gamma oscillations for sensors located over parietal regions (PDM: 48–66 Hz, VDM: 46–64 Hz, $P_{Bonferroni} < 0.001$) (Figures 3B, 3C, 3E, and 3F). Additionally, we found that only for VDM trials, gamma activity of sensors over fronto-polar regions reflected the model-predicted EA signals (46–62 Hz, $P_{Bonferroni} < 0.001$) (Figures 3B and 3E). The same held for beta-band oscillations (18–20 Hz, $P_{Bonferroni} < 0.001$) at fronto-central electrodes during VDM trials, but this time with an inverted relationship (i.e., a negative correlation) (Figures 3A and 3D). For PDM trials, by contrast, our analysis strategy did not reveal any frontal cluster with such oscillatory signals, even at a very liberal statistical threshold ($P_{uncorrected} < 0.001$; please note that null relationships cannot be formally confirmed with classical statistics).

For the second step of the analysis, we tested the model predictions in these identified clusters out of sample by regressing the corresponding time-frequency decompositions of the second half of the data (odd-numbered trials) from these clusters on the model predictions. We found that for all sensor-frequency clusters depicted in Figures 3A–3F, the model predictions were indeed confirmed by the independent data ($R > 0.93$, $p < 10^{-15}$ for all clusters) (Figure 3G). This shows that the model-derived EA signals could indeed accurately predict the temporal shape of gamma power oscillations in the identified regions for fully independent data.

In a second analysis, we tested whether the model predictions also held for the independent dataset when we considered the data extracted from the regions separately for different levels of task difficulty and for trials with long and short RTs (relative to the median RT) at each difficulty level (Figure S4). In these analyses, we established that the extracted EEG traces show two important properties of EA signals. First, we found that there was no significant difference in the response-locked threshold of the signals for trials with different RTs or task difficulty, using repeated-measures ANOVAs of the response threshold with the factors difficulty level (easy/hard) and RT level (fast/slow) (Table S1). Second, we showed that the ramping speed of the EEG signals fully conforms with the predictions of the SSM for fast versus slow and hard versus easy trials. For this second result, we analyzed the EEG signals time-locked to stimulus onset. This was a potentially noisier test due to visual potentials evoked by the sudden onset of our stimuli. As predicted by the model, we found that EEG signals in shorter trials ramp up more quickly than the signals in longer trials (Figures S4C and

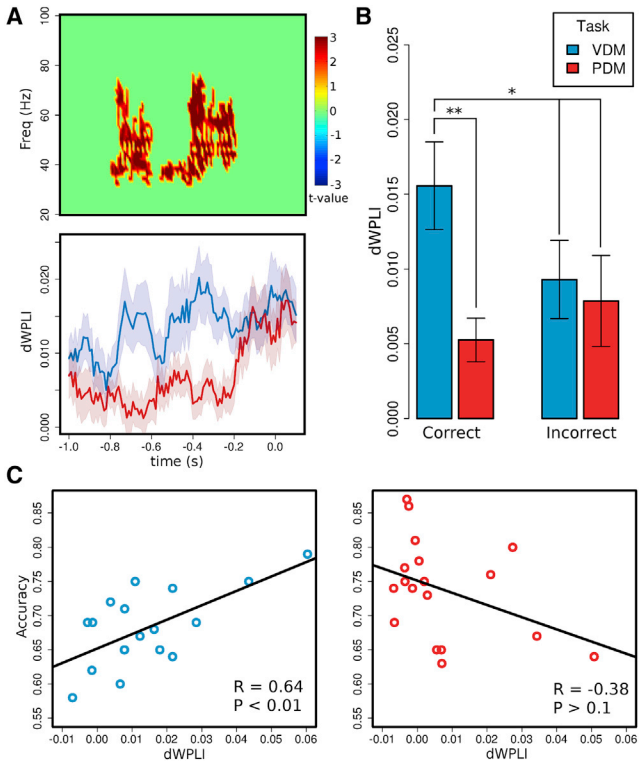

Figure 4. Fronto-Parietal Synchronization

(A) Interregional connectivity (dWPLI) between the fronto-polar sensors shown in Figure 3B and the conjunction of the sensors in parietal clusters shown in Figures 3B and 3C was stronger for VDM than for PDM. Stronger phase-coupling was found for VDM in the ~40–70 Hz frequency range between 0.85 and 0.2 s before response onset (upper plot). Clusters shown in the upper plot survive Monte-Carlo cluster correction for multiple comparisons at $p < 0.05$. Lower plot shows the dWPLI averaged across the 40–70 Hz frequency range for VDM (blue) and PDM (red). Shaded areas represent ±1 SEM.

(B) Fronto-parietal connectivity (dWPLI in the ~40–70 Hz frequency range between 0.85 and 0.2 s before response onset) during VDM (but not PDM) was stronger for correct than for incorrect trials. Error bars represent ±1 SEM. *$p < 0.05$; **$p < 0.01$.

(C) The strength of fronto-parietal connectivity (dWPLI) during VDM correlated with the accuracy of value-based choices. The plot shows linear regressions of mean accuracies for each subject on the dWPLI for each participant in the 45–65 Hz frequency range for latencies between −0.85 and −0.2 ms. This is displayed for VDM (left panel, blue dots) and for PDM (right panel, red dots).

S4D). Additionally, the model predicts marginal differences between easy and hard trials in this analysis (with easier trials ramping up faster than hard trials), which we also observed in our empirical data (Figures S4C and S4E). Together, these results confirm that the EEG signals we identify here indeed show important properties of EA signals predicted by the SSM used in the present study.

In the previous analysis, we investigated the relationship between model and time frequency decompositions independently for VDM and PDM. To test for differences between VDM and PDM, we compared the relationship of model-predicted EA signals and data between conditions (VDM and PDM) by computing a t statistic of correlation differences between conditions across subjects for each EEG channel and each frequency band (Experimental Procedures). This analysis showed that for fronto-polar sensors, the model predictions correlated with oscillations in the gamma-frequency band more strongly for VDM than for PDM ($p < 0.05$ montecarlo cluster-corrected, cluster spanning 48–56 Hz) (Figure 3I). Additionally, we found for sensors located over fronto-central regions that the previously described negative correlation between model-predicted EA signals and beta activity (Figures 3A and 3D) was also stronger for VDM compared to PDM ($p < 0.05$ montecarlo cluster-corrected, cluster spanning 18–25 Hz) (Figure 3H).

Do these differences in neural data relate to differences in behavioral performance (see Figure 1B) between PDM and VDM? To address this issue, we repeated the analysis with performance-matched sets of data. To this end, we compared easy trials in VDM (difficulty level 3 and 4) with difficult trials in PDM (difficulty level 1 and 2), given that accuracies and RTs were not significantly different between these trials ($T(17) < 1.74$, $p > 0.1$; see Figure 1B). Importantly, we were able to reproduce the results obtained in Figures 3H and 3I (see Figure S3). Thus, differences in task difficulty—as measured with RTs and accuracies—cannot explain why model-predicted EA signals showed a stronger correlation with frontal gamma and beta oscillations for VDM than for PDM.

Large-Scale Synchronization of Distributed EA Processes

The finding that both parietal and frontal oscillations related to EA signals for VDM led us to hypothesize that VDM may require the sharing of information between fronto-polar and parietal regions. To test this, we compared the coherence between these two regions by computing the debiased weighted phase lag index (dWPLI). Note that this method ensures that differences in absolute power of oscillations between VDM and PDM cannot affect differences in the degree of coherence between the two conditions (Supplemental Experimental Procedures).

Strikingly, we found that synchrony between parietal and fronto-polar regions was significantly higher for VDM than for PDM in the same gamma frequency range, as identified in the power-modulation analysis (−0.8 to −0.2 s and frequency window between ~40–70 Hz) (see Figure 4A). To ensure that this observed difference in connectivity between VDM and PDM was not caused by differences in task difficulty and/or RTs, we again compared the connectivity measures between easy trials in VDM and difficult trials in PDM. These trials were fully matched for behavior between PDM and VDM (see Figure 1B); however, the connectivity measure between these two types of choice still showed a significant difference ($T(17) > 3.1$, $p < 0.01$) for the same frequency range and latencies as before. The stronger fronto-parietal gamma-band coherence for VDM therefore probably reflects differences in choice processes rather than simply different levels of behavioral performance.

It is often argued that phase synchronization between different sites serves to facilitate communication between segregated cortical areas (Polanía et al., 2012b; Siegel et al., 2012). If both the frontal and parietal oscillations observed here serve an essential but distinct role for VDM, then we should see that the

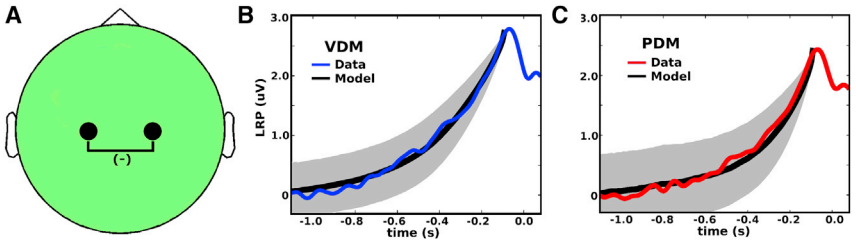

Figure 5. Lateralized Readiness Potential

(A) Simplified schematic representation of how the lateralized readiness potential (LRP) is calculated. Raw electric potentials of sensors located over the left and right motor cortex are subtracted from one another.

(B and C) Shown is the LRP (multiplied by −1 for visualization purposes) for VDM ([B], blue trace) and PDM ([C], red trace) together with model-predicted activity (black). The grey shaded area represents the SD interval of the model prediction. Motor preparatory activity also closely followed the decision variable predicted by the model, suggesting that the LRP may also reflect EA processes. See also Figure S4.

level of gamma-band synchrony between fronto-polar and parietal regions should relate to the level of task performance in VDM. A post hoc analysis indeed revealed that phase coupling between fronto-polar and parietal sensors in the VDM trials was positively correlated with accuracy in VDM trials (linear regression: $r = 0.64$, $p < 0.01$; nonparametric Spearman's correlation: $R_{Spearman} = 0.79$, $p = 0.034$) (left plot in Figure 4C). Conversely, the same phase coupling between fronto-polar and parietal sensors in the PDM trials did not correlate with PDM accuracy (linear regression: $r = -0.39$, $p = 0.11$; nonparametric Spearman's correlation: $R_{Spearman} = -0.38$, $p = 0.12$) (right plot in Figure 4C), and the correlations of synchronization and accuracy correlations were significantly larger for VDM than for PDM ($Z = 3.25$, $p < 0.005$; Supplemental Experimental Procedures). In addition to these correlations across participants, we also tested for a relationship between fronto-parietal synchrony and accuracy at the single-trial level. To this end, we compared our fronto-parietal synchrony measure between correct and incorrect trials for PDM and VDM (repeated measures ANOVA with factors task [PDM/VDM] and accuracy [correct/incorrect]). Fronto-parietal synchrony was significantly stronger for VDM than PDM (main effect task, $F(1,17) = 4.52$ and $P = 0.04$), and this effect was modulated by accuracy at trend level (interaction of task and accuracy, $F(1,17) = 3.69$ and $p = 0.071$) (see Figure 4B). Planned comparisons showed that fronto-parietal synchrony was indeed higher for correct than incorrect trials during VDM trials ($T(17) = 2.41$, $p = 0.02$) but not during PDM trials ($T(17) = 0.9$, $p > 0.3$). Moreover, the synchrony measure during correct VDM trials was higher than during all other trial types (all $T > 2.35$; all $p < 0.05$). These results confirm that fronto-parietal gamma synchrony is related to behavioral performance during VDM.

Relation of Oscillatory EA Signal to Motor Preparatory Activity

The readiness potential (RP) or *Bereitschaftpotential* refers to the slow (1–2 s) buildup of electrical activity over motor-related areas that reliably precedes self-initiated movements. The RP has been proposed as a signature of planning, preparation, and initiation of volitional acts. It has been recently established that for self-initialized movements RPs can be explained as an accumulation-like process (Schurger et al., 2012). However, the involvement of this electrophysiological signature in EA for PDM or VDM, rather than just self-generated responses, is unclear (although see (Gluth et al., 2013a) for a recent study investigating RPs in VDM). Our results revealed that lateralized RPs (LRPs) (Figure 5A) in both PDM and VDM tasks were highly correlated with model predictions of our SSM ($r > 0.95$; $p < 10^{-16}$) (Figures 5B and 5C), therefore supporting suggestions that LRPs may also reflect evidence-accumulation processes (Schurger et al., 2012).

Subsequently, we investigated the relationship between these LRPs and the previously described gamma activity that reflected the model-predicted EA. First we asked whether there was a systematic latency between the peaks in activity of the two signals. Across participants, no such latency was found ($T(17) < 1.1$, $p > 0.3$). Second, we computed the cross-correlation between gamma activity and LRPs in order to investigate whether one of the signals preceded the other as they were drifting towards their maximum. We found that across participants, the lag latency of the cross-correlation peak did not significantly differ from zero ($T(17) < 0.4$, $p > 0.7$). These results suggest that both gamma activity in integrator regions and LRPs follow the EA signals predicted by the OU model in a quasi-parallel fashion. Note that this result does not indicate that gamma activity described in the present study is simply a concomitant of traditionally studied LRPs, but instead that both parietal gamma activity and LRPs may be explained as accumulation-like processes as defined by SSMs (see also Schurger et al., 2012). Future studies should investigate whether these two signals can be dissociated with paradigms that systematically manipulate sensory and motor requirements (see e.g., O'Connell et al., 2012).

DISCUSSION

Our paradigm allowed us to identify common and distinct neural mechanisms of EA in PDM and VDM by explicit comparisons of neural activity during both types of decisions taken on identical stimuli and involving the same motor output. The model-predicted EA signal from a simple SSM accounted for trial-specific gamma power modulations in the parietal cortex for both PDM and VDM tasks and in fronto-polar cortex for just the VDM task. Activity in these parietal and fronto-polar regions was more synchronized in VDM than in PDM, and the degree of synchronization predicted accuracy in VDM, but not in PDM. This pattern of results suggests that parietal regions encode a common decision variable in both PDM and VDM but that frontal regions perform an additional EA process that is unique to value-based decisions. Furthermore, this prefrontal process is coupled

by large-scale interactions with the decision variable encoded in parietal cortex.

What information may be accumulated during the two types of choice? In the PDM task, participants are assumed to decide based on objective color and shape signals that allow the computation and comparison of the physical sizes of the two items (White et al., 2012). In the VDM task, by contrast, it is assumed that decisions are taken based on value signals indicating preference for one item or the other. These signals likely reflect subjective evaluations of the items (Hare et al., 2011; Krajbich et al., 2010; Milosavljevic et al., 2010). Previous work has shown that fixating on an item temporarily boosts the evidence for that item (Krajbich et al., 2010; Towal et al., 2013). In the present task, however, subjects made decisions by covert attention; we therefore cannot provide decisive information as to whether the value signals are partially constructed from attention to the stimuli and/or from memory of prior ratings of the food items. In any case, our use of subjective value differences as inputs to the value-based decision process is fully consistent with prior VDM studies using similar task designs (Milosavljevic et al., 2010; Krajbich et al. 2010, Philiastides and Ratcliff, 2013). Moreover, our model fits clearly suggest that such value-related information is accumulated in a similar fashion as perceptual information during decision making.

The observed monotonic increase of gamma activity in evidence integration regions (as the motor-execution point is approached) may possibly emerge from an evolving amplification of the activity representing the conflicting alternatives, which is generated by synaptic reverberation of NMDA receptors mediated by feedback inhibition (Wang, 2002). These signals represent the coordinated activity of large pools of neurons and can therefore be captured via readout of extracellular electric fields (Buzsáki and Wang, 2012). In humans, this notion is supported by MEG studies suggesting that emerging gamma activity in parietal regions reflects perceptual readout and action planning (Pesaran, 2010; Van Der Werf et al., 2010). Moreover, monotonic increases of high gamma activity—representing accumulation of sensory evidence in PDM—have also been observed in sensorimotor regions (Donner et al., 2009). Here we have shown that such gamma-activity patterns evolve with the temporal shape of EA processes as predicted by the SSM fitted to the observed behavioral data. Moreover, our data demonstrate that these signals are also observed at fronto-polar electrodes during value-based decisions, thus further supporting the idea that medial-frontal regions play a central role in value-based choices and in the accumulation of value-based evidence (Basten et al., 2010; Hare et al., 2011; Harris et al., 2011; Hunt et al., 2012; Lim et al., 2011; McNamee et al., 2013; Philiastides et al., 2010).

In addition to oscillations in the gamma range, we also found that beta oscillations over fronto-central regions negatively followed the predicted EA signal only for value-based decisions. Monotonic decreases of beta oscillations in motor-related areas have often been proposed as a signature of action control and also integration of sensory neural activity for decision making (Donner et al., 2009; Gluth et al., 2013b; de Lange et al., 2013; O'Connell et al., 2012; Wyart et al., 2012). On the other hand, recent theories of frontal cortex contributions to value-guided decision-making suggest that distinct substructures of fronto-central cortex may perform different computations during the decision-making process in parallel; while ventro-medial frontal regions are thought to compute and/or compare the values of the offered alternatives, posterior segments of the anterior cingulate cortex (ACC) and dorso-medial prefrontal cortex (dmPFC) have been proposed to instantiate comparisons of action values (Kolling et al., 2012; Shenhav et al., 2013). These latter computations may involve anatomical connections linking dmPFC and ACC with both supplementary motor areas and areas of the ventro-medial prefrontal cortex (Beckmann et al., 2009). Although the relatively low spatial resolution of EEG recordings does not allow us to infer the involvement of specific prefrontal sites, the ACC and dmPFC are certainly candidate regions that may generate the fronto-central beta-band activity that negatively followed the predicted EA signal, possibly reflecting valuation of the action to be taken (Kolling et al., 2012; Shenhav et al., 2013).

Our findings revealed that value-based EA involves parallel and synchronized frequency-specific oscillations in fronto-polar and parietal regions. Moreover, these processes were accompanied by a buildup of motor preparatory activity, as measured with LRPs in this study. This underlines that multiple neural signals in the shape of EA processes are deployed in parallel during choice. Our finding of such EA signals in frontal, parietal, and motor-related areas is generally in line with previous neuroimaging or electrophysiology studies that have identified such signals separately for each of these areas, as well as the basal ganglia (Ding and Gold, 2013; Donner et al., 2009; Klein-Flügge et al., 2013; O'Connell et al., 2012; Shadlen and Newsome, 2001). One possible explanation for the widespread occurrence of EA signals across different brain areas is that integrators of sensory evidence may be constantly readout in downstream decision regions (e.g., those that assign value to choice options) and ultimately in motor structures through cortico-striatal-thalamo-cortical circuits (Bogacz and Larsen, 2011; Ding and Gold, 2013). These coordinated signals may therefore reflect rapid information transfer between brain regions coding different aspects of sensory or internal evidence that need to be integrated for the choice outcome.

In line with this possibility, we found that coupling between fronto-polar and parietal regions was higher in value-based than in perceptual-based EA and that such synchronization occurred in the same gamma-frequency range in which oscillatory activity in these two regions tracked EA processes. Furthermore, we found that the strength of phase coupling in the gamma band between fronto-polar and parietal regions was crucially related to improved behavior in VDM, whereas it was not relevant for PDM. This may reflect that parietal cortex, proposed to be responsible for perceptual readout of the incoming sensory evidence (Huk and Shadlen, 2005), may share this information with frontal regions that implement valuation and comparison of the offered alternatives (Basten et al., 2010; Hunt et al., 2012; Philiastides et al., 2010). That relative increases of phase coupling occurred in a high frequency band—the same in which evidence was accumulated—may have allowed a rapid transfer of information between remote neural populations (Gregoriou et al., 2009; Siegel et al., 2008). As discussed above, the transfer of information between relatively distant frontal and parietal

regions might be relayed by subcortical regions; however, anatomical dissection studies have also shown that certain regions of the parietal cortex are directly linked with orbito-frontal regions (Cavada et al., 2000), thus also potentially allowing fast large-scale synchronization in the gamma band (Gregoriou et al., 2009).

Our findings appear broadly consistent with recent suggestions of EEG and MEG studies that have also used SSMs as a tool to derive predictions for slow (<10 Hz) oscillatory neural signals in independent studies of either PDM (van Vugt et al., 2012) or VDM (Hunt et al., 2012). However, our study is the first to use predictions of computational models fitted to behavioral data in order to predict an EA signal for both PDM and VDM in fully matched tasks, therefore allowing the comparison of these two types of EA processes.

Taken together, the results of the present study bolster the notion that decisions emerge from an integrative EA process that occurs in parallel across distinct brain regions that process different aspects of the incoming sensory signals (e.g., perceptual and value readout). This process appears to be instantiated locally by neural oscillations and seems to be coordinated between different areas via large-scale neural synchronization. Future studies should explore whether simple accumulator models in conjunction with EEG measures can further identify and distinguish the neural signals related to evidence integration underlying other common types of human decisions, such as social, risky, and intertemporal choices.

EXPERIMENTAL PROCEDURES

Subjects

A total of 23 healthy right-handed volunteers (age 20 to 30) with normal or corrected-to-normal vision were included in the study. Subjects were informed about all aspects of the experiment and gave written informed consent. None of the participants suffered from any neurological or psychological disorder or took medication during the time the experiment was conducted. Subjects were paid 70 CHF for their participation in the experiment, in addition to receiving one food item (see below). The experiments conformed to the Declaration of Helsinki and the experimental protocol was approved by the Ethics Committee of the Canton of Zurich.

Stimuli and Behavioral Task

Subjects were asked not to eat or drink anything within 3 hr before the start of the experiment. After the experiment, subjects were required to stay in the room with the experimenter while eating the food item that they chose in a randomly selected trial of the VDM task (see below).

The behavioral task consisted of two main steps: (1) the rating phase and (2) the decision-making task. In the rating phase, we asked the participants to provide subjective perceptual- and value-based ratings from the same set of 65 different food images using an on-screen slider scale. All of the food items were in stock in our lab, and subjects were notified about this. For value-based ratings, participants indicated "how much they wanted to eat the presented food snack at the end of the experiment" with a scale from −10 to 10 in steps of 1. For perceptual-based ratings, we asked the participants to provide an estimate of "how much (in percent) they thought the food item was covering the black background within the white square" on a scale from 5% to 100% in steps of 5% (see Figure S1). Before providing the ratings, subjects briefly saw all of the items for an effective use of the value-based rating scale.

Immediately after the ratings, an algorithm selected a balanced set of PDM and VDM trials divided in four different difficulty levels based on the individual subjective ratings provided by each participant. Difficulty levels for the VDM task were $r_{best} - r_{worst} \in [1, 2, 3, 4]$ and for PDM were $r_{bigger} - r_{smallest} \in [5\%, 10\%, 15\%, 20\%]$. Afterwards, subjects proceeded to perform the decision-making task. Trials started with presentation (for 2 s) of a central fixation cross (~0.2°) and a word (length ~0.8°; height ~0.3°) indicating whether subjects were in a PDM trial (word "LIKE") or in a VDM trial (word "AREA"). On the subsequent screen, the fixation cross was replaced by the letter "L" or "A" (~0.2°) to remind subjects that they were in a VDM or PDM trial, respectively. Over this cue letter, an additional cue symbol (either ">" or "<"; both ~0.2°) instructed subjects to covertly shift attention to the right or left visual fields, respectively. Subjects were instructed to keep their eyes fixated on the central cue for at least 1.5 s (this was controlled by the use of eye tracking, see below). Only after successful fixation for at least 1.5 s were the two food items simultaneously displayed at the right or left side of the screen (x eccentricity: 4.3°; y eccentricity: 3.6°; white square surrounding each food item, width 6°) (see Figure 1A), as indicated by the prior cue. Simultaneously, an average-scrambled image of the two food items was displayed on the opposite side of the screen (see Figure 1A) in order to avoid spatial imbalance in the display, therefore preventing reflexive saccades as observed in pilot experiments.

In the VDM task, subjects indicated which item (upper or lower) they would prefer to receive at the end of the experiment while in the PDM task, subjects indicated which item (upper or lower) covered more area within the white square. To make these choices, subjects used a key-pad button located under their right-index finger (upper item) or the right thumb (lower item). During the decision period, subjects were instructed not to generate eye-blinks and to make the decision by covert attention (see eye-tracking below). Subjects had 4 s to make a decision; otherwise the trial was marked as a "miss trial". We defined a correct choice as a trial in which the subject chose the item with a higher rating from the separate rating tasks. Each experimental session consisted of 480 trials divided in eight blocks of 60 trials each. The maximum number of consecutive PDM or VDM trials in a single block was pseudo-randomized to between 6 and 12 trials. The 480 trials were fully balanced across all factors (visual field [left/right]; trial type [PDM or VDM]; difficulty level [1–4]; correct response [up/down]).

EEG Recordings

EEGs were recorded against an average reference electrode using sintered Ag/AgCl electrodes at 128 positions with an equidistant hexagonal layout using a Waveguard Duke 128 channels cap (http://www.ant-neuro.com/) connected to a 128-channel QuickAmp system (Brain Products). Electrode impedance was monitored throughout the experiment to be below 10 KΩ. Sampling frequency rate was 512 Hz at an analogue-digital precision of 24 bits. The EEG cap was set up on each subject's head before participants proceeded to the soundproof and electromagnetically shielded chamber to perform the ratings and the decision-making task during EEG recordings.

Eye Tracking

Subjects' fixation patterns were tracked and recorded at 500 Hz with an EyeLink-1000 (http://www.sr-research.com/). Before each choice trial, subjects were required not to blink and maintain fixation at the center of the screen for 1.5 s before the items would appear. Afterwards the food items were displayed (see above). From stimulus onset until the response was detected, subjects were also required not to blink and maintain fixation (tolerance 1.2°), otherwise the trial was aborted and subjects received a feedback message indicating that the trial was interrupted due to eye movements. Such trials were marked as "invalid" in our behavioral and EEG analyses. Subjects practiced the task and fixation in a 10 min practice session of the decision-making task. For this practice session, subjects were presented with a different set of stimuli than those used in the real experimental session.

Behavioral Analysis

RTs and accuracies were split into VDM and PDM trials and averaged separately for each of the four difficulty levels described above (see Figure 1B). To investigate the effects of the PDM and VDM on RTs in correct trials, we constructed the following linear regression model:

$$RT_{correct} = \beta_0 + \beta_1 OV + \beta_2 VD + \beta_3 SD + \beta_4 OS. \quad (2)$$

We defined r_i and a_i as the subjective value rating and area rating of each food image i, respectively. For any given trial, we define $OV = r_{image1} + r_{image2}$, $VD = r_{best} - r_{worst}$, $SD = a_{biggest} - a_{smallest}$, and $OS = a_{image1} + a_{image2}$ (see Figure 1C). This model was independently fitted for each subject and each experimental condition (PDM or VDM).

To investigate the effects of PDM and VDM tasks on accuracies, we constructed the following logistic regression model:

$$P_{choice} = \frac{1}{1 + \exp(-(\beta_0 + \beta_1 OV + \beta_2 VD + \beta_3 RT + \beta_4 SD + \beta_5 OS))}, \quad (3)$$

where in addition to the already defined *OV*, *VD*, *SD*, and *OS* (see above), *RT* denotes the RT in the current trial. This model was independently fitted for each subject and each experimental condition (PDM or VDM).

After fitting these models for each subject and each experimental condition, parameter estimates were standardized and their deviance from 0 was estimated with a two-sided t test (see Figures 1C and 1D).

Computational Model

As our SSM approach, we used the general form of the one-dimensional OU process. The OU is described by the following equation:

$$dEA = (\lambda \times EA + kI)dt + \sigma dW, \quad (1 \text{ in main text})$$

where I is the input to the system (i.e., difference in value or relative size between the food items), k is a parameter that scales the input, λ is a parameter that denotes the leak strength (or urgency) of the process and serves as an adaptive control mechanism that can directly shape evidence integration computation (Bogacz et al., 2006; Brunton et al., 2013), and σdW are independent white noise (Wiener) increments of step σ. We used $dt = 0.001$ s, and we assumed that the model makes a decision when $|x| \geq 1$. Additionally, we accounted for visual processing and cortico-muscular responses by subtracting a non-decision time (*nDT*, a free parameter to be fitted) from the empirical RTs.

The model was fit to the RT data separately for correct and incorrect trials in order to account for both RTs and choice accuracies. Initially, we fitted the model to the individual data of each participant and compared the fitted parameters for the two decision types (Figure S2A). In order to derive the model-predicted EA signal for the EEG analyses, we then fitted the model to the data pooled across participants to ensure the maximum amount of precision for parameter estimation (Figure S2B). The data were fit to the model using maximum likelihood estimation. RTs were separated for VDM and PDM trials into correct/incorrect trials for each of the four difficulty levels, and the *nDT* was subtracted from these data. These RT distributions were compared to the distributions generated by the model. For a given set of values of model parameters, we estimated the log likelihood (*LL*) of the data using the following formula:

$$LL = \sum_{i_{correct}=1}^{4} \log\left(KS\left(RT^i_{Data}, RT^i_{Model}\right)\right) + \sum_{i_{incorrect}=1}^{4} \log\left(KS\left(RT^i_{Data}, RT^i_{Model}\right)\right), \quad (4)$$

where *KS(x,y)*, is the probability that two distributions are equal, estimated with the Kolmogorov-Smirnov test, and i represents a given difficulty level. Then, we identified the set of parameters of the model that maximized the log likelihood. The search was performed over a coarse grid search of values for λ = [−9, −8.8,…, 8.8, 9], k = [0,0.005, …, 0.3], σ = [0.02, 0.04, …, 1.5] and nDT = [0.2, 0.25, …, 0.6] s. The simulation of the model for each set of parameters at a given point of the grid was run with 5,000 simulations.

We used these fitted parameters to generate model-predicted EA signals by averaging activity of 5,000 trials time-locked to the decision latencies starting −1.1 s before the decision threshold is crossed (see Figure 2). If the response time of the model was shorter than −1.1, then we padded the beginning of the epoch with null values (i.e., these values did not contribute to the average across simulated trials). Averages of model-predicted activity were quantitatively and qualitatively tested against the average time-frequency decompositions of our collected EEG data (see below).

EEG Analysis

Analysis of the data was performed using a custom-built script implemented in Matlab 7.12 64-bit (The MathWorks) and Fieldtrip (Oostenveld et al., 2011). EEG datasets were divided into epochs starting 1.3 s before response and finishing 0.3 s after response. In the present study, there are two main reasons to focus our analyses on response-locked EEG signals: (1) typically, RTs were greater than 1 s; therefore, response-locked analyses allow us to minimize contamination from early visual evoked potentials, and (2) SSMs—like the OU process—do not predict activity after the decision is made; thus, response-locked analyses allow us to exclude these data. Line noise was removed using discrete Fourier transform, and all trials were first cleaned from artifacts. This was initially done using independent component analysis to identify eye movements and other noise artifacts. Note that our valid trials are free of eye blinks (see eye tracking above). Careful inspection of the individual components was based on topography and power spectrum to remove components representing artifacts. Furthermore, individual trials were visually inspected, and those with extremely high variance (e.g., muscle artifacts) were removed from the data. Two subjects were excluded from further analysis due to excessive artifacts. Three additional subjects were removed from the analysis due to excessive invalid trials (i.e., trials with eye blinks or saccades over 50%; see eye tracking above). Thus, all of the analyses in this study (behavior, models, and EEG) were carried out with the remaining 18 subjects. For these remaining subjects, on average, 18% ± 4.3% of the trials were rejected.

Spectral estimates were performed for each correct trial based on a multitaper method using standard routines implemented in Fieldtrip. Analyses were performed in the 16–100 Hz frequency range. The length of the temporal sliding window was exactly eight cycles per time window in steps of 0.02 s. The width of frequency smoothing was set to $0.3 \times f$ with a frequency resolution in steps of 1 Hz. We characterized power relative to a prestimulus baseline −0.5 to −0.1. For each EEG channel and experimental condition (VDM or PDM), the spectral estimates were averaged across trials and subjects. The time decomposition of each frequency and each channel was correlated with the activity predicted by the model. Correlations were computed from −1.2 s to −0.1 s with respect to response detection. The reason for placing the leading end of the model at −100 ms is that this point has been shown to coincide with an abrupt increase in cortico-spinal excitability; activity after that time is therefore likely attributable to motor execution per se rather than choice and response preparation (Chen et al., 1998; Gratton et al., 1988; Haggard, 2011).

We inspected the EEG data for the model-predicted EA signals with a data analysis strategy that combined qualitative and quantitative criteria (see below). This strategy was essential as we are not interested in any possible monotonic relationship between model and data, but only in oscillatory signals that closely follow model-predicted EA signals. Trials were divided into even and odd trials in order to test predictions of the fitted model out of sample (i.e., against independent data). To this end, we first used the even-numbered trials to identify sensors where oscillatory activity was closely related the shape of the model-predicted EA signal; we then formally tested the model predictions against the data from the independent odd-numbered trials. The analysis for the first half of the data was carried out in two steps: first, a linear regression with 55 time points in each time series (i.e., −1.2 to −0.1 s in steps of 0.02 s) was calculated between time-frequency decompositions of the actual even-numbered trials and model predictions. We only considered sensors belonging to frequency-spatial clusters that survived Bonferroni correction at $p < 0.05$. Second, from the sensor-frequency clusters surviving the quantitative tests, we only further considered time-frequency decompositions in sensor space that lay within 1 SD of the model predictions to ensure that fits were based on the full temporal interval. Afterwards, in order to test our model predictions out of sample, we investigated the relationship between model and the second half of the data (linear regression between model and odd-numbered trials) based on the sensor-frequency clusters identified in the previous analysis.

To compare the relationship of model predictions and data between conditions (e.g. between VDM and PDM), we computed a t statistic of the difference

in correlation ($r_{Pearsons}$) between model predictions and data for each EEG channel and each frequency band. Initially, we thresholded the 3D (2D topographic location of the electrodes + frequency) two-sided t statistic map at $p < 0.05$. For each cluster surviving this threshold, we defined its size as the integral of the t scores (condition difference) across the extension of the cluster and tested its significance using a permutation statistic (i.e., we repeated the cluster identification 10,000 times with shuffled condition labels to create an empirical distribution of cluster sizes under the null hypothesis of no difference between conditions) (Maris, 2012). Here we report clusters surviving a cluster correction for multiple comparisons at $p < 0.05$.

SUPPLEMENTAL INFORMATION

Supplemental Information includes four figures, one table, and Supplemental Experimental Procedures and can be found with this article online at http://dx.doi.org/10.1016/j.neuron.2014.03.014.

ACKNOWLEDGMENTS

We thank Todd A. Hare for his helpful comments and Gabor Stefanics for his valuable help in setting up the EEG lab. This work was supported by grants of the SNSF (105314_152891, CRSII3_141965, and 51NF40_144609) and the SNSF NCCR Affective Sciences to C.C.R.

Accepted: February 21, 2014
Published: May 7, 2014

REFERENCES

Basten, U., Biele, G., Heekeren, H.R., and Fiebach, C.J. (2010). How the brain integrates costs and benefits during decision making. Proc. Natl. Acad. Sci. USA *107*, 21767–21772.

Beckmann, M., Johansen-Berg, H., and Rushworth, M.F. (2009). Connectivity-based parcellation of human cingulate cortex and its relation to functional specialization. J. Neurosci. *29*, 1175–1190.

Bode, S., Sewell, D.K., Lilburn, S., Forte, J.D., Smith, P.L., and Stahl, J. (2012). Predicting perceptual decision biases from early brain activity. J. Neurosci. *32*, 12488–12498.

Bogacz, R., and Larsen, T. (2011). Integration of reinforcement learning and optimal decision-making theories of the basal ganglia. Neural Comput. *23*, 817–851.

Bogacz, R., Brown, E., Moehlis, J., Holmes, P., and Cohen, J.D. (2006). The physics of optimal decision making: a formal analysis of models of performance in two-alternative forced-choice tasks. Psychol. Rev. *113*, 700–765.

Bollimunta, A., and Ditterich, J. (2012). Local computation of decision-relevant net sensory evidence in parietal cortex. Cereb. Cortex *22*, 903–917.

Bowman, N.E., Kording, K.P., and Gottfried, J.A. (2012). Temporal integration of olfactory perceptual evidence in human orbitofrontal cortex. Neuron *75*, 916–927.

Brunton, B.W., Botvinick, M.M., and Brody, C.D. (2013). Rats and humans can optimally accumulate evidence for decision-making. Science *340*, 95–98.

Buzsáki, G., and Wang, X.J. (2012). Mechanisms of gamma oscillations. Annu. Rev. Neurosci. *35*, 203–225.

Buzsáki, G., Anastassiou, C.A., and Koch, C. (2012). The origin of extracellular fields and currents—EEG, ECoG, LFP and spikes. Nat. Rev. Neurosci. *13*, 407–420.

Cavada, C., Compañy, T., Tejedor, J., Cruz-Rizzolo, R.J., and Reinoso-Suárez, F. (2000). The anatomical connections of the macaque monkey orbitofrontal cortex. A review. Cereb. Cortex *10*, 220–242.

Chen, R., Yaseen, Z., Cohen, L.G., and Hallett, M. (1998). Time course of corticospinal excitability in reaction time and self-paced movements. Ann. Neurol. *44*, 317–325.

Churchland, A.K., Kiani, R., and Shadlen, M.N. (2008). Decision-making with multiple alternatives. Nat. Neurosci. *11*, 693–702.

de Lange, F.P., Rahnev, D.A., Donner, T.H., and Lau, H. (2013). Prestimulus oscillatory activity over motor cortex reflects perceptual expectations. J. Neurosci. *33*, 1400–1410.

Deco, G., Rolls, E.T., and Romo, R. (2010). Synaptic dynamics and decision making. Proc. Natl. Acad. Sci. USA *107*, 7545–7549.

Ding, L., and Gold, J.I. (2013). The basal ganglia's contributions to perceptual decision making. Neuron *79*, 640–649.

Donner, T.H., and Siegel, M. (2011). A framework for local cortical oscillation patterns. Trends Cogn. Sci. *15*, 191–199.

Donner, T.H., Siegel, M., Fries, P., and Engel, A.K. (2009). Buildup of choice-predictive activity in human motor cortex during perceptual decision making. Curr. Biol. *19*, 1581–1585.

Gerstner, W., Sprekeler, H., and Deco, G. (2012). Theory and simulation in neuroscience. Science *338*, 60–65.

Gluth, S., Rieskamp, J., and Büchel, C. (2013a). Classic EEG motor potentials track the emergence of value-based decisions. Neuroimage *79*, 394–403.

Gluth, S., Rieskamp, J., and Büchel, C. (2013b). Deciding not to decide: computational and neural evidence for hidden behavior in sequential choice. PLoS Comput. Biol. *9*, e1003309.

Gold, J.I., and Shadlen, M.N. (2007). The neural basis of decision making. Annu. Rev. Neurosci. *30*, 535–574.

Gratton, G., Coles, M.G., Sirevaag, E.J., Eriksen, C.W., and Donchin, E. (1988). Pre- and poststimulus activation of response channels: a psychophysiological analysis. J. Exp. Psychol. Hum. Percept. Perform. *14*, 331–344.

Gregoriou, G.G., Gotts, S.J., Zhou, H., and Desimone, R. (2009). High-frequency, long-range coupling between prefrontal and visual cortex during attention. Science *324*, 1207–1210.

Haggard, P. (2011). Decision time for free will. Neuron *69*, 404–406.

Hare, T.A., Schultz, W., Camerer, C.F., O'Doherty, J.P., and Rangel, A. (2011). Transformation of stimulus value signals into motor commands during simple choice. Proc. Natl. Acad. Sci. USA *108*, 18120–18125.

Harris, A., Adolphs, R., Camerer, C., and Rangel, A. (2011). Dynamic construction of stimulus values in the ventromedial prefrontal cortex. PLoS ONE *6*, e21074.

Huk, A.C., and Shadlen, M.N. (2005). Neural activity in macaque parietal cortex reflects temporal integration of visual motion signals during perceptual decision making. J. Neurosci. *25*, 10420–10436.

Hunt, L.T., Kolling, N., Soltani, A., Woolrich, M.W., Rushworth, M.F., and Behrens, T.E. (2012). Mechanisms underlying cortical activity during value-guided choice. Nat. Neurosci *15*, 470–476.

Kelly, S.P., and O'Connell, R.G. (2013). Internal and external influences on the rate of sensory evidence accumulation in the human brain. J. Neurosci. *33*, 19434–19441.

Kiani, R., and Shadlen, M.N. (2009). Representation of confidence associated with a decision by neurons in the parietal cortex. Science *324*, 759–764.

Kim, J.N., and Shadlen, M.N. (1999). Neural correlates of a decision in the dorsolateral prefrontal cortex of the macaque. Nat. Neurosci. *2*, 176–185.

Klein-Flügge, M.C., Nobbs, D., Pitcher, J.B., and Bestmann, S. (2013). Variability of human corticospinal excitability tracks the state of action preparation. J. Neurosci. *33*, 5564–5572.

Kolling, N., Behrens, T.E., Mars, R.B., and Rushworth, M.F. (2012). Neural mechanisms of foraging. Science *336*, 95–98.

Krajbich, I., and Rangel, A. (2011). Multialternative drift-diffusion model predicts the relationship between visual fixations and choice in value-based decisions. Proc. Natl. Acad. Sci. USA *108*, 13852–13857.

Krajbich, I., Armel, C., and Rangel, A. (2010). Visual fixations and the computation and comparison of value in simple choice. Nat. Neurosci. *13*, 1292–1298.

Lim, S.L., O'Doherty, J.P., and Rangel, A. (2011). The decision value computations in the vmPFC and striatum use a relative value code that is guided by visual attention. J. Neurosci. *31*, 13214–13223.

Maris, E. (2012). Statistical testing in electrophysiological studies. Psychophysiology *49*, 549–565.

McNamee, D., Rangel, A., and O'Doherty, J.P. (2013). Category-dependent and category-independent goal-value codes in human ventromedial prefrontal cortex. Nat. Neurosci. *16*, 479–485.

Milosavljevic, M., Malmaud, J., Huth, A., Koch, C., and Rangel, A. (2010). The drift diffusion model can account for value-based choice response times under high and low time pressure. Judgement Decis. Mak. *5*, 437–449.

O'Connell, R.G., Dockree, P.M., and Kelly, S.P. (2012). A supramodal accumulation-to-bound signal that determines perceptual decisions in humans. Nat. Neurosci. *15*, 1729–1735.

Oostenveld, R., Fries, P., Maris, E., and Schoffelen, J.M. (2011). FieldTrip: Open source software for advanced analysis of MEG, EEG, and invasive electrophysiological data. Comput. Intell. Neurosci. *2011*, 156869.

Ossmy, O., Moran, R., Pfeffer, T., Tsetsos, K., Usher, M., and Donner, T.H. (2013). The timescale of perceptual evidence integration can be adapted to the environment. Curr. Biol. *23*, 981–986.

Pesaran, B. (2010). Neural correlations, decisions, and actions. Curr. Opin. Neurobiol. *20*, 166–171.

Philiastides, M.G., and Ratcliff, R. (2013). Influence of branding on preference-based decision making. Psychol. Sci. *24*, 1208–1215.

Philiastides, M.G., Biele, G., and Heekeren, H.R. (2010). A mechanistic account of value computation in the human brain. Proc. Natl. Acad. Sci. USA *107*, 9430–9435.

Polanía, R., Paulus, W., and Nitsche, M.A. (2012a). Noninvasively decoding the contents of visual working memory in the human prefrontal cortex within high-gamma oscillatory patterns. J. Cogn. Neurosci. *24*, 304–314.

Polanía, R., Nitsche, M.A., Korman, C., Batsikadze, G., and Paulus, W. (2012b). The importance of timing in segregated theta phase-coupling for cognitive performance. Curr. Biol. *22*, 1314–1318.

Ratcliff, R., Cherian, A., and Segraves, M. (2003). A comparison of macaque behavior and superior colliculus neuronal activity to predictions from models of two-choice decisions. J. Neurophysiol. *90*, 1392–1407.

Ratcliff, R., Philiastides, M.G., and Sajda, P. (2009). Quality of evidence for perceptual decision making is indexed by trial-to-trial variability of the EEG. Proc. Natl. Acad. Sci. USA *106*, 6539–6544.

Schurger, A., Sitt, J.D., and Dehaene, S. (2012). An accumulator model for spontaneous neural activity prior to self-initiated movement. Proc. Natl. Acad. Sci. USA *109*, E2904–E2913.

Shadlen, M.N., and Newsome, W.T. (2001). Neural basis of a perceptual decision in the parietal cortex (area LIP) of the rhesus monkey. J. Neurophysiol. *86*, 1916–1936.

Shenhav, A., Botvinick, M.M., and Cohen, J.D. (2013). The expected value of control: an integrative theory of anterior cingulate cortex function. Neuron *79*, 217–240.

Siegel, M., Donner, T.H., Oostenveld, R., Fries, P., and Engel, A.K. (2008). Neuronal synchronization along the dorsal visual pathway reflects the focus of spatial attention. Neuron *60*, 709–719.

Siegel, M., Donner, T.H., and Engel, A.K. (2012). Spectral fingerprints of large-scale neuronal interactions. Nat. Rev. Neurosci. *13*, 121–134.

Smith, P.L., and Ratcliff, R. (2004). Psychology and neurobiology of simple decisions. Trends Neurosci. *27*, 161–168.

Summerfield, C., and Tsetsos, K. (2012). Building bridges between perceptual and economic decision-making: neural and computational mechanisms. Front. Neurosci. *6*, 70.

Towal, R.B., Mormann, M., and Koch, C. (2013). Simultaneous modeling of visual saliency and value computation improves predictions of economic choice. Proc. Natl. Acad. Sci. U S A *110*, E3858–E3867.

Usher, M., and McClelland, J.L. (2001). The time course of perceptual choice: the leaky, competing accumulator model. Psychol. Rev. *108*, 550–592.

Van Der Werf, J., Jensen, O., Fries, P., and Medendorp, W.P. (2010). Neuronal synchronization in human posterior parietal cortex during reach planning. J. Neurosci. *30*, 1402–1412.

van Vugt, M.K., Simen, P., Nystrom, L.E., Holmes, P., and Cohen, J.D. (2012). EEG oscillations reveal neural correlates of evidence accumulation. Front. Neurosci. *6*, 106.

Wang, X.J. (2002). Probabilistic decision making by slow reverberation in cortical circuits. Neuron *36*, 955–968.

White, C.N., Mumford, J.A., and Poldrack, R.A. (2012). Perceptual criteria in the human brain. J. Neurosci. *32*, 16716–16724.

Wyart, V., de Gardelle, V., Scholl, J., and Summerfield, C. (2012). Rhythmic fluctuations in evidence accumulation during decision making in the human brain. Neuron *76*, 847–858.